

Investigation of the Saturation of Elemental Concentration in the Depth Profile of Low Energy Silver Ion Implants in Silicon

MANGAL S. DHOUBHADEL, BIBHUDUTTA ROUT*,
WICKRAMAARACHCHIGE J. LAKSHANTHA, FLOYD D. McDANIEL*

Ion Beam Modification and Analysis Laboratory, Department of Physics, University of North Texas, Denton, Texas 76203, USA

*Email: bibhu@unt.edu, mcaniel@unt.edu

Published online: August 08, 2016,

The Author(s) 2016. This article is published with open access at www.chitkara.edu.in/publications

Abstract For the efficient absorption of light in a broad wavelength band, Si photovoltaic devices require a high concentration of metal atoms at a shallow depth up to a few 10s of nm in the Si substrates. Low energy (< 50 keV) implantation of Ag ions in Si is one of the most suitable synthesis steps to facilitate the formation of these metal nanoclusters at the shallow depths in Si. However, during the low energy implantation of the heavy ions, one of the unintended consequences is the sputtering of target atoms particularly if the target is made of lower Z materials such as Si. In this study, we have investigated the re-distribution of atoms in the target layers due to the surface sputtering effects from 50 keV Ag ion implantation in Si substrates. Initially, the implant profile was estimated with the widely used static simulation code, the Stopping and Range of Ions in Matter (SRIM). However, its simulation routine lacks any consideration of the fluence dependent evolution of the target material. Therefore, we have explored the use of another ion-solid interaction code T-DYN, which considers the dynamic changes in the thickness and/or composition of the target material during the implantation process. For 50 keV Ag ion implantation in Si, the T-DYN simulation predicts the Ag ion depth profile reaches a maximum or saturation in the concentration at a critical ion fluence of $\sim 7 \times 10^{16}$ atoms/cm², whereas for a more heavier element like Au, similar saturation in the concentration is predicted at a relatively lower fluence of $\sim 4 \times 10^{16}$ atoms/cm². The depth profiles of the implanted Ag atoms extracted from experiments utilizing the Rutherford Backscattering Spectrometry and X-ray Photoelectron Spectroscopy characterization techniques show

Journal of Nuclear
Physics, Material
Sciences, Radiation and
Applications
Vol-4, No-1,
August 2016
pp. 251–264

Dhoubhadel, M.S.
Rout, B.
Lakshantha, W.J.
McDaniel, F.D.

asymmetric distributions with the position of peak concentration depth gradually moving towards the Si surface with increasing implant ion fluence. Once the implantation ion fluence reached a critical value, the peak value of the elemental concentration is seen saturated similar to the predictions from T-DYN simulations.

Keywords: Ag nanoclusters; ion implantation; depth profile; RBS; XPS

1. INTRODUCTION

The understanding of the interaction of light with metal nanoclusters (NC) has given rise to a wide range of applications, such as photovoltaic (PV) devices, optical sensors, and optical emitters [1-3]. In last several decades, it has been understood that the embedded metal NC in a dielectric matrix plays an important role in optoelectronic applications [1-2]. The metal-dielectric interface can generate surface plasmons (SP) [4]. The metal NC can also excite the SP and doing so increases the optical path length in the PV layer without increasing the physical thickness of the PV to enhance overall photo absorption [5]. The characteristics of optical absorption due to the metal NC depend on the size, geometry, species and location in the dielectric media or substrate [6]. Metal NC such as Ag can enhance the light absorption and increase the efficiency of PV device [7-8]. Pillai et al. had demonstrated the enhancement in quantum efficiency after integrating metal nanoparticles (NPs) on thin polycrystalline silicon solar cells with ~30nm spacer layer [8]. Shi et al. had shown that light trapping can be enhanced by fabricating double layer Ag nanoparticles in silicon based materials [9]. Recently, Sardana et al. had reported the necessity of an optimized SiO_2 spacer layer of 20-30 nm between the metal NPs and silicon solar cell for enhancing forward scattering from the NPs into the silicon substrate in the long wavelength region [10].

The absorption depth of the light of different wave lengths is different in Si [6, 11], so placing the NC according to its size plays a critical role in improving the device efficiency [3, 12]. For the efficient absorption of light in a broad wavelength band, Si photovoltaic devices require a high concentration of dopant metal atoms or NC such as Ag at a shallow depth of a few 10s of nm in the Si substrates. Low energy (< 50 keV) implantation of Ag ions in Si is one of the most suitable synthesis steps to facilitate the formation of the metal nanostructures at the shallow depths in Si. The metallic NCs nucleate spontaneously when the implanted ion fluence exceeds the solubility saturation point [13]. The spontaneous nucleation from the direct ion irradiation produces homogeneous NC in size and location; however, the probability of NC nucleation is small. The threshold thermodynamic energy for NC nucleation

is often higher than the energy provided by ion implantation process. The formation of the metal NC and their graded distribution in the dielectric layers can be achieved by further in-situ or post-thermal annealing of the substrate [14]. Recently Seo et al. have reported the formation of Ag NC at the Si surface using 50 keV Ag ion implantation at a high current density of $5\text{mA}/\text{cm}^2$ and a total fluence of $\sim 2 \times 10^{17}$ atoms/ cm^2 with post-thermal annealing at 400°C [15]. The thermal annealing increases the probability of NC nucleation, but the NC size and their distribution are very much dependent on the fluence and energy (range and distribution) of the implanted ions in the substrate.

However, during the low energy implantation of the heavy ions, one of the unintended consequences is the sputtering of target atoms particularly if the target is made of lower Z materials such as Si. The sputtering yield is a function of target surface binding energy, element type, implantation energy, and other irradiation parameters. It is extremely important to know how the energetic ion modifies the target substrate in order to design a device with tailored NCs at certain depths. As an example, Figure 1, shows the sputtering effects on a Si target from the implantation of 76 keV Ag at a fluence of 5×10^{15} atoms/ cm^2 . Earlier, Liau et al. had estimated the sputtering yield of Au, Cu and Si by 45 keV ions of various atomic numbers up to $Z=90$ [16]. In the high-fluence ion implantation process, the maximum concentration of the implanted atom or compositional ratio with the target atoms is determined by the amount of ion induced sputtering yield of the implanted layer.

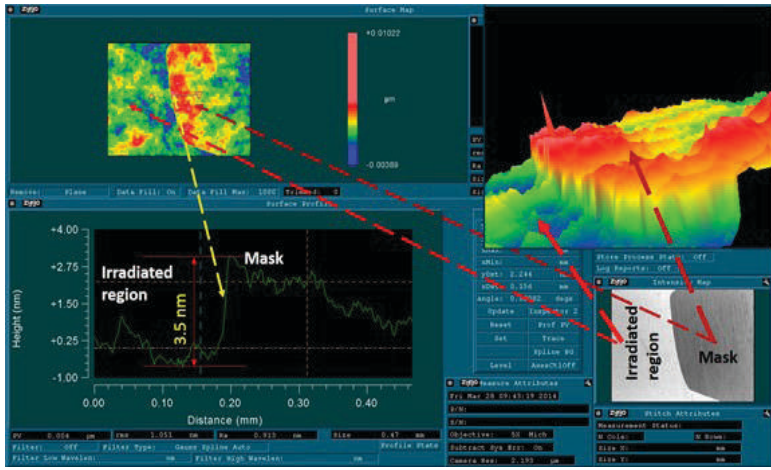


Figure 1: 76 keV Ag ions were implanted with a fluence 5×10^{15} atoms/ cm^2 in Si. The Ag ion implantation induced sputter etched ~ 3.5 nm of the Si surface layer. This surface topology map was acquired using a Zygo optical surface profilometer.

Dhoubhadel, M.S.
Rout, B.
Lakshantha, W.J.
McDaniel, F.D.

In the present paper, we have investigated the re-distribution of atoms in the target layers due to the surface sputtering effects from low energy (50 keV) Ag ions implanted in the Si substrate. Initially, the implant profile was estimated using the widely used static TRIM/ SRIM simulation code [17]. The static code provides the number of surface atoms sputtered per incident ion and the changes in the incident energy due to this sputtering process. However, it's simulation routine lacks any consideration of the fluence dependent evolution of the target materials. Therefore, we have explored the use of another ion-solid interaction code T-DYN, which considers the dynamic changes in the thickness and/or composition of target materials during the implantation process [18-21]. Rutherford Backscattering Spectrometry (RBS) and X-ray Photoelectron Spectroscopy (XPS) techniques were used to characterize the ion implant concentration depth profile in the experimental samples.

2. EXPERIMENTAL

Single crystal Si (100) (Boron doped p-type, resistivity of 10–20 Wcm) wafers were irradiated with 50 keV energy Ag⁺ ions at fluences ranges from $\sim 1 \times 10^{16}$ atoms/cm² to $\sim 1 \times 10^{17}$ atoms/cm². The ion source for the ion implantation was a National Electrostatic Corporation (NEC) SNICS II (source of negative ion by cesium sputtering), which is one of the three sources attached to a NEC 3 MV tandem (9SDH-2 Pelletron) accelerator [22]. The ion implantation was carried out in the low energy (LE) implant line before the tandem accelerator. The beam was electrostatically raster scanned over a circular aperture to homogeneously implant an area of 3.14 cm². The current density for the ion implantation was maintained at less than one $\mu\text{A}/\text{cm}^2$ to minimize the self-annealing of the implanted sample. All the samples were tilted to $\sim 7^\circ$ to the surface normal to avoid ion channeling. During the implantation, the residual gas pressure in the experimental chamber was $\sim 2 \times 10^{-7}$ mbar. The RBS measurements were carried out using a rectangular collimated beam ($\sim 1 \text{ mm}^2$) of 2.0 MeV He⁺ ions from a single ended 3 MeV accelerator (NEC, 9SHPelletron) [22]. The RBS detector was placed at a scattering angle of 150°. The angle of beam incidence with respect to the sample surface normal was fixed at 6°. To minimize the secondary electrons, the He⁺ ion beam passes through a series of aperture and ceramic disc magnets just at the opening of the analyzing chamber along with a negative 300 volt electron suppressor at the grid where the charge is being integrated. The charges were integrated at a tungsten wire mesh installed in the beam line right after the slit [23]. The RBS spectra were analyzed with the SIMNRA computer package [24]. Corresponding depth profiles were extracted from the RBS spectra. The thickness of a 10 nm Ag thin film used

as a standard for RBS measurements was monitored by a crystal monitor installed in the thermal evaporating chamber. A ZygoNewView™ 7300 optical profilometer was also used to measure the thickness of the Ag standard sample as well as the edge of the sputtered layer (shown in Figure 1). X-ray photoelectron spectroscopy (XPS) measurements were performed with a PHI 5000 Versaprobe. Al monochromatic X-ray radiation (1486.6 eV) was focused to a spot size of about 200 μm . The pressure of the analysis chamber was kept initially at 5×10^{-10} mbar. In this system, the full width at half maximum (FWHM) of the Ag 3d_{5/2} peak was ≤ 0.50 eV for the energy range 372 eV to 365 eV. The XPS depth profiling measurements were performed with Ar ion sputtering. The sputtering was performed with a 2 keVAr beam of 2 μA current exposing an area of 3×3 mm². The Ar ion sputtering rate was calibrated to be 4 nm per minute for a SiO₂ standard sample. The XPS measurements were performed at the Center for Advanced Research and Technology (CART) facility of UNT.

3. RESULTS AND DISCUSSION

3.1. *Simulation of Sputtering of Target atoms and Implant ion distributions*

The TRIM ion-solid interaction simulation code, can provide a statistical distribution of the implanted ions in the target matrix. Along with the statistical ion distribution, using the full cascade damage option, TRIM calculates the damage, ion vacancies, and ion sputtering yield in the target layer. The TRIM calculation was performed for 100,000 incident ions and the results were normalized to higher fluences. The TRIM calculations predict that the 50 keV Ag ion at the angle of 7° has a sputtering yield of ~3.2 Si atoms per Ag ion. The sputtering yield of Si for Ag atoms at 10 keV is ~ 1 Si atom/ion and gradually reaches a maximum at ~ 50 keV, where most of the ion-atom interactions occur predominantly in the nuclear energy loss region. The projected range of the 50 keV Ag ions in Si is ~33 nm with a straggling of ~9.8 nm. The number of sputtered atoms from the target layer become significant at the high fluences and the dynamic changes of the implanting target layer during the ion irradiation is quite significant. However, the TRIM simulation routine lacks any direct consideration of the fluence dependent evolution of the target materials. Therefore, to study the dynamic modification of the target layer during the high fluence ion interactions, we have used another ion-solid interaction code, T-DYN, which considers the dynamic changes in the thickness and/or composition of the target materials during the implantation process. The T-DYN code is based on the static TRIM program using the binary collision approximation (BCA) for ballistic transport. It allows inclusion of up

Dhoubhadel, M.S.
Rout, B.
Lakshantha, W.J.
McDaniel, F.D.

to five different atomic species in the target and/or in the incident beam to be considered, with different energies and angles of incidence for the implantation. It is capable of predicting the depth profiles of all atomic species in the target as a function of fluence of the incident projectiles. Additionally, the sputtering yields, total areal densities, surface concentrations and re-emitted amounts are calculated as a function of fluence, as well as the surface erosion. For the T-DYN simulations, an area size of $10\text{ nm} \times 10\text{ nm}$ with a Si target depth of 100 nm were considered and the simulations were performed separately for various ion fluences.

In Figure 2(a) the T-DYN simulation plots for 50 keV Ag ions of fluences ranging from $1 \times 10^{16}\text{ atoms/cm}^2$ to $1 \times 10^{17}\text{ atoms/cm}^2$ are presented. The TRIM data for the 50 keV Ag with a fluences of $1 \times 10^{16}\text{ atoms/cm}^2$ and $2 \times 10^{16}\text{ atoms/cm}^2$ are also presented in the same figure for comparison. We have also compared T-DYN and TRIM simulations for even heavier implants such as Au. In Figure 2(b), similar T-DYN simulated data carried out for the 50 keV Au ions irradiating Si along with TRIM data are presented. Note, that as the fluence becomes larger, the centroid of the implant moves closer to the surface, indicating that the surface is being sputtered away during the implantation process. At about $\sim 3 \times 10^{16}\text{ atoms/cm}^2$, the implanted Ag as well as Au ions are seen at the top surface layers of the Si substrate due to the excessive sputtering of the target atoms and the implanted ions. Also, it is interesting to note that the implant ion concentrations reach a saturation value after reaching a critical fluence. In Figure 3, the amount of Ag and Au ions retained in the Si matrix as a function of fluence is shown. For the 50 keV Ag ions, the saturation in the concentration is seen at a fluence of ~ 6 to $7 \times 10^{16}\text{ atoms/cm}^2$. For the 50 keV Au ions, the saturation in the concentration is seen at $\sim 4 \times 10^{16}\text{ atoms/cm}^2$. In the case of Au implanted samples, there is a slight increase in the Au concentration in the surface region (first 4 nm) due to a higher sputtering rate of Si than of Au at the surface layers. This might be useful in growing self-assembled heavy metal nanostructures on the surfaces of Si substrates based on the underlying symmetry of the Si (100), (110) and (111) substrates [25-26].

3.2 Experimental Depth Profiles of the implanted ions using RBS and XPS Characterization Techniques

In Figure 4 (a), the RBS spectra from samples implanted with various fluences of 50 keV Ag are shown. The incremental trend in the Ag peak area (between 1680 keV - 1740 keV) indicates the corresponding increments in the Ag implantation fluences. The peak with the black solid line is from the RBS standard sample of 10 nm thick Ag thermally deposited on Si. The thickness

Investigation of
the Saturation
of Elemental
Concentration in
the Depth Profile of
Low Energy Silver
Ion Implants in
Silicon

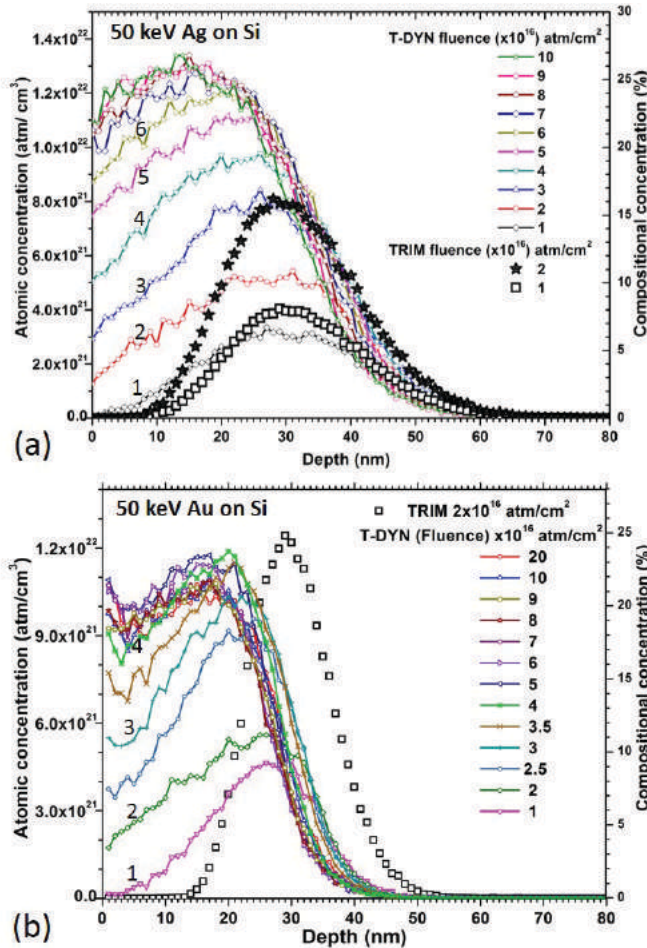


Figure 2: T-DYN simulation of 50 keV (a) Ag and (b) Au ion implantation in Si matrices. The data from the TRIM simulations for the fluences of 1×10^{16} atoms/cm 2 and 2×10^{16} atoms/cm 2 are also presented for comparison.

of the 10 nm Ag thin film used as a thickness standard was monitored by a crystal monitor installed in the thermal evaporation chamber. Also, the Ag layer thickness was verified by the optical profilometer. The leading Ag edge in the RBS spectra is approximately at 1731 keV. The leading Ag edges of the high fluence peaks are about the same as the standard sample. However, for the Ag peaks with lower fluences, the leading edges are well below the 1731 keV indicating the Ag is scattering from atoms located below the surface of the sample, as the surface has not been sputtered away as much at the lower

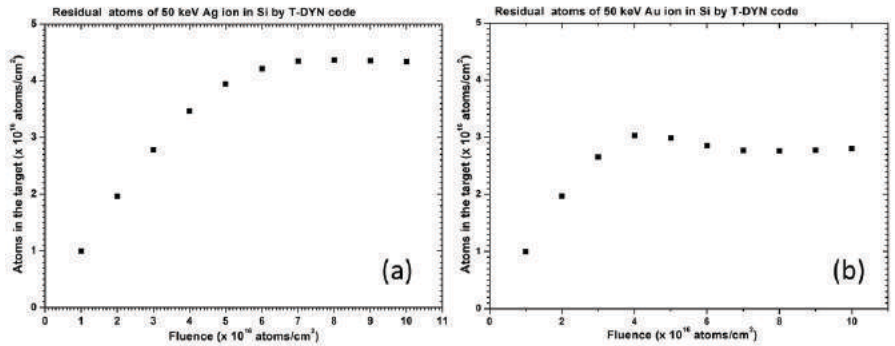


Figure 3: (a) The T-DYN simulations showing the Ag retained in the Si matrix for the various Ag implantation fluences. The Ag ion concentration starts to saturate at ~ 6 to 7×10^{16} atoms/cm 2 . (b) The Au retained in the Si matrix vs the implanted Au fluence in Si as simulated with the T-DYN code. The Au ion concentration starts to saturate at ~ 3 to 4×10^{16} atoms/cm 2 .

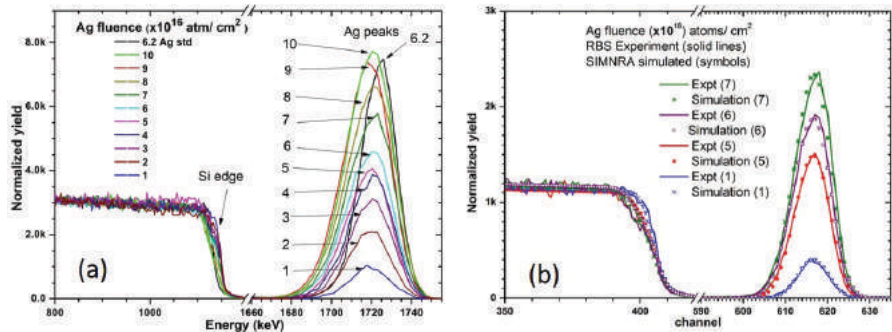


Figure 4: (a) RBS Spectra of 50 keV Ag implanted in the Si (100) matrix with the fluence ranges from 110^{16} atoms/cm 2 to 110^{17} atoms/cm 2 . A 10 nm (~ 6.2 atoms/cm 2) Ag thin film deposited on Si was taken as standard to calibrate the Ag signal. (b) Selected RBS Spectra along with fitted spectra simulated using the SIMNRA analysis code.

fluences. The Si leading edge at 1146 keV is from the surfaces of the virgin Si. The Ag fluence of 1×10^{17} atoms/cm 2 will sputter 3.19×10^{17} Si atoms/cm 2 , which is about 88 nm thick of Si. For this fluence, the Si edge is at 1122 keV, which is shifted by 24 keV. The slope of the Si edge for the 1×10^{17} atoms/cm 2 sample is more gradual and has a step at the lower edge, which is due to the enrichment of the Ag ions from the ion irradiation and the Si concentration is decreased at this region. The leading Ag edge from samples with fluences

4×10^{16} atoms/cm² and higher starts at (or very close to) 1731 keV, indicating the location of Ag atoms at the surface of the implanted samples.

In order to extract quantitative depth profiles of the Ag implanted ions, the RBS spectra were analyzed by using the SIMNRA code. The Ag ion implanted layer is modelled as several layers of single thin films of homogeneous mixtures of Ag and Si. The Ag compositional profile was extracted by dividing the target layer up into approximately 20 layers with equal depth intervals. Figure 4(b) shows some of the selected RBS spectra along with corresponding SIMNRA analyzed fitted spectra from the Ag implanted samples. In Figure 5, the depth profiles of the Ag atoms in the various implanted samples as extracted from the RBS spectra using the SIMNRA simulation package are shown. The implanted ions follow the same general trend in the T-DYN simulations shown in Figure 2(a).

Figure 6 (a), shows the Ag XPS spectra as a function of Ar sputtering time/ sequence for 50 keV Ag implanted into Si with a fluence of 7×10^{16} atoms/

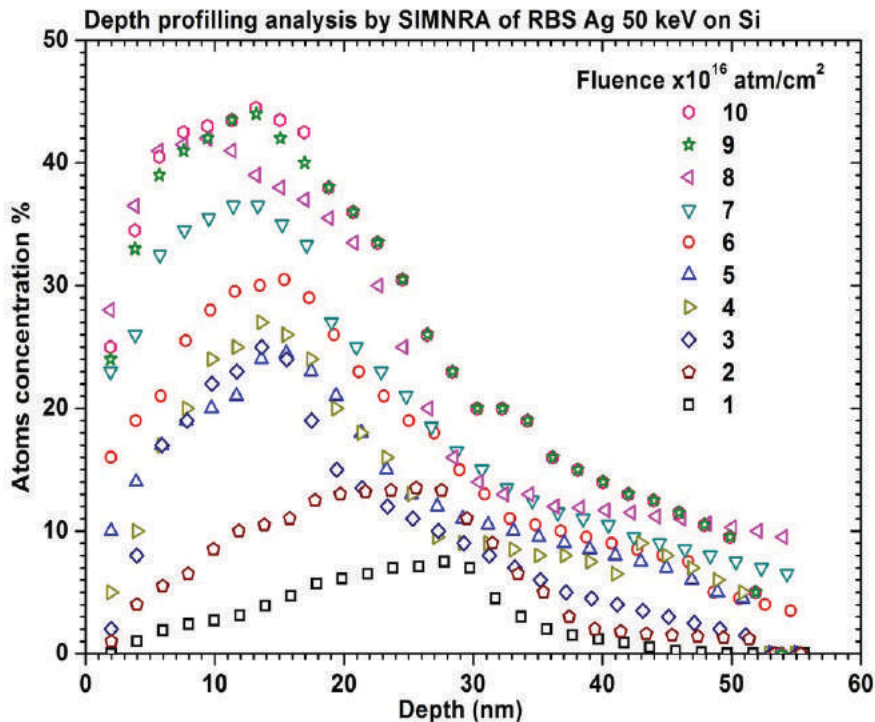


Figure 5: Depth profile of Ag atoms extracted from the RBS spectra of 50 keV Ag implanted Si samples (as shown in Figure 4) using the SIMNRA package.

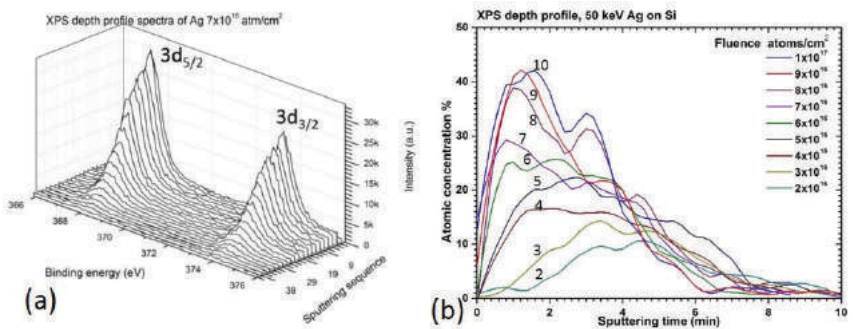


Figure 6: (a) Ag XPS spectra as a function of Ar sputtering time/sequence of 50 keV Ag implanted into Si with a fluence of 7×10^{16} atoms/cm². The Ag $3d_{3/2}$ peak at 373.5 eV was integrated at each sequence to extract the concentration depth profiles. (b) Depth profile of Ag atomic concentration extracted from the XPS spectra of samples with different fluences of Ag implantation into Si.

cm². The Ag XPS peaks, $3d_{5/2}$ at 367.5 eV and $3d_{3/2}$ at 373.5 eV, show gradual changes for different Ar sputtering cycles. The Ag $3d_{3/2}$ peak at 373.5 eV, after suitable background subtraction, was integrated at each sequence to extract the concentration depth profiles of the Ag implanted samples. The concentration depth profiles of the Ag atoms in the various implanted samples extracted from the XPS spectra as a function of Ar ion sputtering time are shown in Figure 6 (b). The depth profiles show similar distribution trends as the T-DYN and SIMNRA simulated profiles. For the higher implantation fluences on the Si samples, the Ag concentration profiles show more localized Ag atom distributions at 3 minutes of Ar etching interval.

From both RBS and XPS analysis, the atomic concentrations of Ag atoms were found to be slightly higher in the Si substrate than the T-DYN simulations for the higher implantation fluences. The highest (saturation) concentration predicted from the T-DYN is about 26 % for the Ag. The T-DYN simulations also predict the self-sputtering of Ag at the lower fluences, for example, at the fluence of 1×10^{16} atoms/cm², Ag sputtered away about 0.1 % of the Ag implants and at the higher fluence of 1×10^{17} atoms/cm², Ag is predicted to sputter ~56.7% of the Ag implants. It appears that, the experimental results are consistent with results reported by several other groups working with 30–50 keV Ag ion implantation in Si. In one of our earlier studies for 50 keV Fe implanted in Si with a fluence 2×10^{17} atoms/cm², the Fe profiles from RBS and XPS also showed the Fe concentration in the substrate to be more than 50%, whereas the T-DYN profiles calculated about 42% concentration [21, 27]. In

the article by Seo et al., the saturated Ag concentration retained in the Si target for 50 keV energy implantation with a fluence of 1×10^{17} atoms/cm² is found to be ~33% atomic concentration [15]. Though the T-DYN code considers the dynamic changes in the distribution of the target atoms, it doesn't incorporate conditions for possible alloy formation or inter-diffusion between target atoms due to ion beam mixing or the increase in the local (nanometer length scale) temperatures during the ion implantation process. The alloy formation and/or diffusion of the heavy ions to deeper layers can contribute to higher retention concentrations of the implants. For the 32 keV Au ion implantation in Si, Sahu et al., had observed Au concentration saturation after the implantation fluence reached $\sim 4 \times 10^{16}$ atoms/cm² [28]. For the 40 keV Ag implantation in Si with a fluence of 1×10^{17} atoms/cm², Sahu et al. had observed retention of more than 60 % of the implanted Ag ions, which was explained in the light of higher diffusion constant of Ag in Si than Au in Si.

4. CONCLUSIONS

At the higher fluences, the depth profiles of the implanted atoms predicted from the T-DYN simulations clearly depart from the well-known static TRIM simulation. The Ag ions concentration profiles starting from the fluence of 7×10^{16} atoms/cm² and higher shows the Ag ion saturation in the silicon target. The T-DYN analysis in figure 3 clearly shows the critical fluence for the implant ion concentration saturation is around 7×10^{16} atoms/cm² for Ag ions implanted in the silicon substrate. The concentration depth profiles extracted from RBS and XPS follow similar trends. It appears that the total sputtering yield from the target is compensated by the implanted ions and the total Ag ion concentration does not increase after it exceed the saturation point. The presence of Ag at the surface of the Si are starting to appear from the fluence of 3×10^{16} atoms/cm² in the XPS depth profile spectra. The understanding of the target sputtering and concentration saturation for heavy ion implants in Si offers an excellent opportunity to design top-down fabrication processes for synthesis of multi-dimensional metal NC in buried layers of Si with precise accuracy in depth as well as atomic concentration. For the designing of staggered Ag NC in Si, the energy of the successive ion implantation has to be widely separated to compensate for the atom sputtering from the ion implantation.

5. ACKNOWLEDGEMENTS

The authors would like to thank Dr. Matthias Posselt from the Institute of Ion Beam Physics and Materials Research, Helmholtz-Zentrum Dresden-

Dhoubhadel, M.S.
Rout, B.
Lakshantha, W.J.
McDaniel, F.D.

Rossendorf, Germany for providing the latest version of the T-DYN simulation code. We would like to thank the CART facility at UNT for the use of XPS characterization equipment.

REFERENCES

- [1] Guo, ChuanFei, Sun, Tianyi, Cao, Feng, Liu, Qian, and Ren, Zhifeng, Metallic nanostructures for light trapping in energy-harvesting devices, *Light: Science & Applications*,3, e161(2014); doi:10.1038/lsta.2014.42. <http://dx.doi.org/10.1038/lsta.2014.42>
- [2] Pillai, S., Green, M. A. (2012), Plasmonics for Photovoltaics, Reference Module in Earth Systems and Environmental Sciences –Comprehensive Renewable Energy, A. Sayigh (Ed.) Vol 1: Photo-voltaic Solar Energy, (pp. 641-656), Oxford: Elsevier Ltd.
- [3] Garcia,M. A., Surface plasmons in metallic nanoparticles: fundamentals and applications, *J. Phys. D: Appl. Phys.*,44, 283001 (2011). <http://dx.doi.org/10.1088/0022-3727/44/28/283001>
- [4] Stockman,M. I.,Nanoplasmonics: The physics behind the applications, *Phys. Today*,64 (2), 39-44 (2011). <http://dx.doi.org/10.1063/1.3554315>
- [5] Ferry,Vivian E.,Sweatlock,Luke A.,Pacifici, Domenico and Atwater,Harry A., Plasmonic Nano-structure Design for Efficient Light Coupling into Solar Cells, *Nano Lett.*, 8(12), 4391-4397 (2008). <http://dx.doi.org/10.1021/nl8022548>
- [6] Kelly,K. Lance,Coronado,Eduardo,Zhao,Lin Lin and Schatz,George C.,The Optical Properties of Metal Nanoparticles: The Influence of Size, Shape, and Dielectric Environment,*J. Phys. Chem.*,107 (3), 668 (2003). <http://dx.doi.org/10.1021/jp026731y>
- [7] Atwater,Harry A. Polman,Albert,Plasmonics for improved photovoltaic devices, *Nature Materials*,9, 205 (2010). <http://dx.doi.org/10.1038/nmat2629>
- [8] Pillai,S.,Beck,F. J., Catchpole, K. R., Ouyang, Z., Green,M. A., The effect of dielectric spacer thickness on surface plasmon enhanced solar cells for front and rear side depositions, *J. Appl. Phys.*,109, 073105 (2011). <http://dx.doi.org/10.1063/1.3567299>
- [9] Shi,Yanpeng, Wang,Xiaodong, Liu, Wen, Yang, Tianshu, Xu, Rui, and Yang, Fuhua, Multilayer silver nanoparticles for light trapping in thin film solar cells, *J. Appl. Phys.*,113, 176101 (2013). <http://dx.doi.org/10.1063/1.4801785>
- [10] Sardana, Sanjay K., Komarala, Vamsi K.,Influence of SiO₂ Spacer Layer Thickness on Performance of Plasmonic Textured Silicon Solar Cell, *Plasmonics*, (2016), DOI 10.1007/s11468-016-0209-2. <http://dx.doi.org/10.1007/s11468-016-0209-2>
- [11] Green, Martin A. and Keevers, Mark J., Optical properties of intrinsic silicon at 300 K, *Progress in Photovoltaics: Research and Applications*, 3(3) 189-192 (1995), John Wiley & Sons, Ltd. <http://dx.doi.org/10.1002/pip.4670030303>

Investigation of
the Saturation
of Elemental
Concentration in
the Depth Profile of
Low Energy Silver
Ion Implants in
Silicon

- [12] Krishnan, A., Das, S., Krishna, S. R., Khan, M. Z. A., Multilayer nanoparticle arrays for broad spectrum absorption enhancement in thin film solar cells, Opt. Express, 22 A800–A811 (2014). <http://dx.doi.org/10.1364/OE.22.00A800>
 - [13] Meldrum, A., Haglundjr., R. F., Boatner, L. A., White, C. W., Nanocomposite Materials Formed by Ion Implantation, Adv. Mater., 13 (19), 1431-1444 (2001). [http://dx.doi.org/10.1002/1521-4095\(200110\)13:19<1431::AID-ADMA1431>3.0.CO;2-Z](http://dx.doi.org/10.1002/1521-4095(200110)13:19<1431::AID-ADMA1431>3.0.CO;2-Z)
 - [14] ‘Mangal S. Dhoubhadelet al.’, Investigation of structural and optical properties of Ag nanoclusters formed in Si(100) after multiple implantations of low energies Ag ions and post-thermal annealing at a temperature below the Ag-Si eutectic point, AIP Conf. Proc., 1607, 16-23 (2014). <http://dx.doi.org/10.1063/1.4890698>
 - [15] ‘H. W. Seo et al.’, Formation of Silver nanoparticles in silicon by metal vapor vacuum arc ion im-plantation, Nucl. Instru. and Meth. in Phys. Res., B 292, 50-54 (2012).
 - [16] Liau, Z. L. and Mayer, J. W., Limits of composition achievable by ion implantation, J. Vac. Sci. Technol., 15(5), 1629 (1978). <http://dx.doi.org/10.1116/1.569820>
 - [17] J. F. Ziegler, Stopping and range of ions in matter, SRIM-2013, the latest version is available at <http://www.srim.org/>.
 - [18] Wolfgang Eckstein, “Computer Simulation of Ion-Solid Interactions”, Springer Series in Materials Science, v10 (1991). Springer, Berlin. <http://dx.doi.org/10.1007/978-3-642-73513-4>
 - [19] Möller, W., Eckstein, W. and Biersack, J. P. TRIDYN – Binary Collision Simulation of atomic col-lisions and dynamic composition changes in solids, Comput. Phys. Commun., 51, 355-368, (1988). The latest version of the T-DYN package is available at <http://www.hzdr.de/db/Cms?pNid=0&pOid=21578>.
 - [20] Mutzke, A., Schneider, R., Eckstein, W., Dohmen, R., MPI for Plasma Physics, SDTrimSP: Version 5.00., IPP Report 12/8 (2011).
 - [21] Lakshantha,Wickramaarachchige J.,Kummari,Venkata C., Reinert, Tilo, McDaniel, Floyd D., Rout, Bibhudutta,Depth profile investigation of β -FeSi₂ formed in Si(100) by high fluence implantation of 50 keV Fe ion and post-thermal vacuum annealing, Nucl. Inst. and Meth., B 332, 33-36(2014).
 - [22] ‘B. Rout et al.’, An Overview of the Facilities, Activities, and Developments at the University of North Texas Ion Beam Modification and Analysis Laboratory (IBMAL), AIP Conf. Proc., 1544, 11(2013). <http://dx.doi.org/10.1063/1.4813454>
 - [23] ‘M. El Bouanani et al.’, Simple and accurate spectra normalization in ion beam analysis using a transmission mesh-based charge integration, Nucl. Inst. and Meth., B243 (2), 392-396 (2006).
 - [24] An analysis program for RBS analysis, SIMNRA version 6.06 by Matej Mayer. The latest version is available at: <http://home.rzg.mpg.de/~mam/>.
 - [25] ‘S. Chakraborty et al.’, Shape variation in epitaxial microstructures of gold silicide grown on Br-passivated Si(111) surfaces, Surf. Sci., 549 (2), 149-156 (2004). <http://dx.doi.org/10.1016/j.susc.2003.11.034>
-

-
- Dhoubhadel, M.S.
Rout, B.
- Lakshantha, W.J.
McDaniel, F.D.
-
- [26] ‘B. Rout et al.’, Self-assembled gold silicide wires on bromine-passivated Si(110) surfaces, J. of Vac. Sci. and Tech.,B 18(4), 1847-1852(2000).
- [27] Lakshantha, Wickramaarachchige J., Dhoubhadel, Mangal S., Reinert, Tilo, McDaniel, Floyd D., Rout, Bibhudutta, Investigation of Fe-Si phase structures formed in Si by low energy Fe ion im-plantation, Nucl. Inst. and Meth.,B365, 114-119 (2015). <http://dx.doi.org/10.1016/j.nimb.2015.07.037>
- [28] Sahu, G., Rath, S. K., Joseph, B., Roy, G. S., Mahapatra, D. P., Saturation effects observed in high fluence heavy ion implantation at few tens of keV, Vacuum,83, 836-840 (2009). <http://dx.doi.org/10.1016/j.vacuum.2008.08.005>